

QUANTITATIVE ESTIMATION OF SUSPENDED PARTICULATE MATTER FROM CHRIS IMAGES

Suhyb Salama and J. Monbaliu

Hydraulics lab KULeuven, Kasteelpark Arenber 40, 3001 Heverlee, Belgium

ABSTRACT

This paper highlights the utility of standard hyperspectral techniques and algorithms to retrieve useful information from CHRIS imagery. The end-objective being the demonstration of CHRIS capability in retrieving marine bio-geophysical quantities. The major conclusion of this present study is that CHRIS-imagery, in its present status, can be used for operational retrieval of marine bio-geophysical quantities within reasonable accuracy. Though improvements are still needed to enhance the quality of the retrieved products.

Key words: SPM.

1. INTRODUCTION

Suspended particulate matter (SPM) is an important environmental indicator for geomorphological change, pollution, primary production and climate change. The knowledge on SPM loads, spatial distributions and physical properties is essential to maintain navigational routes and to monitor coastal morphology. Sediments in suspension are capable of transporting loads of adsorbed nutrients, pesticides, heavy metals, and other toxins and decreasing the light penetration into the water. This affects fish feeding, photosynthesis and water temperature. The last two phenomena have a direct link to the climate change. Data acquired by the Compact High Resolution Imaging Spectrometer (CHRIS) mounted on PROBA satellite provide wealth of information on the spatial, temporal and angular distribution of SPM in the Belgian coastal waters.

The processing of CHRIS images was subdivided

into three phases namely, pre-processing, retrieval and validation. The objective of the pre-processing was to retrieve accurate values of the water leaving reflectance. This was realized through noise removal, georeferencing, atmospheric correction and vicarious calibration. Marine biogeophysical quantities were then retrieved in the second processing-phase of CHRIS images. The results were validated with in-situ measurements. The post-processing phase will encompass improving the quality of retrieved parameters using hyperspectral and multi-viewing capabilities of CHRIS sensor.

1.1. Site description

The study area is the Belgian coastal water. This water-region is extremely shallow with a depth ranging from 2 to less than 30 meters. The area is under strong meteorological forcing and tidal current. The combined effects of strong motion and shallow water result in a vertically homogeneous water column. The Belgian coastal water, therefore, exhibits a permanent high load of suspended matter reaching 40 g.m^{-3} off the coast and may increase (especially in the winter off Oostende) to more than 100 g.m^{-3} Eisma & Kalf (1979). This high load of suspended sediment arises from transport and re-suspension of sediment materials through hydrodynamic processes, from river discharge and from the nearly continuous dredging activities in the area.

1.2. Characteristics of the Sensors

The operational mode of CHRIS was set to 1 (table 1), i.e. 62 spectral bands distributed on the

range between $0.4 \mu\text{m}$ and $1.05 \mu\text{m}$ with 30meter spatial resolution.

Table 1. The operational mode of CHRIS sensor.

Parameter	CHRIS
Dynamic range [bit]	12
FOV [°]	± 1.3
spectral range [μm]	0.4-1.05
Number of bands	62
Spatial resolution [m]	30
flight altitude [km]	645
SNR	200: 0.2

2. PRE-PROCESSING

2.1. De-stripping and noise removal

Prominent vertical striping was evident in all CHRIS images. This might be due to the difference in noise level (and thus calibration) between adjacent detectors. This difference in calibration arises because each vertical column represents the sequential output of a single detector. The minimum noise fraction (MNF) transforms was employed to remove noise including vertical stripes from data Green et al. (1988). This was by performing a forward transform, determining which bands contain the coherent images, and running an inverse MNF transform using a spectral subset to include the noise free bands only. An example is shown for a CHRIS image acquired on the 05th of August with FZA=+36. This image was de striped using the first three components of the forward MNF (figure 1).

From figure (1) we can observe that the MNF transform has retained the spatial distribution of the blue band while removing the stripe and other noise including some spikes (e.g. ship induced waves). One can argue that using the first three eigen modes, only, to perform inverse MNF transform will lead to losses in the data which have high frequency in a similar manner to a low-pass filter. In other words, some of the information will be lost in the inverse procedure of the MNF transform. However a high frequency signal, surrounded by low water-signals, arises from either an object floating on the water surface (e.g boat, buoy etc.), sun glint or whitecaps. It is of importance for water studies to remove these signals

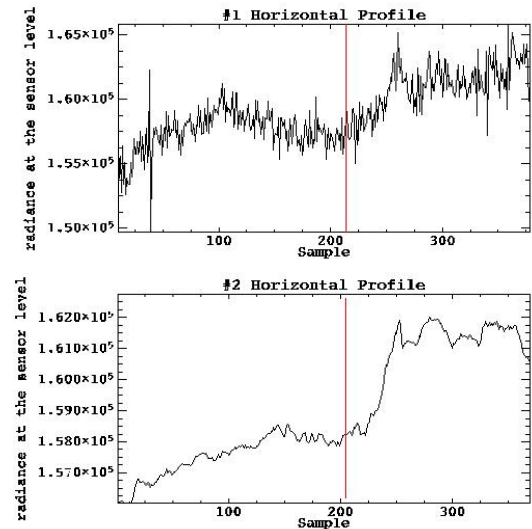


Figure 1. above: Horizontal profile in the original image at the blue band $0.41 \mu\text{m}$. below: the same transection as the above panel after de striping using the first three eigen-modes.

to get reliable results. Still to what degree (i.e. number of the eigen-modes used in the inverse) the MNF will contribute in whitening the data, this will be left to future investigations.

2.2. Geo-referencing CHRIS image using ground control points

Number of ground control points (GCP) were extracted from a cartographical map which were visible on CHRIS images. These GCP were then used to perform the geometric correction. The results are shown for a CHRIS image acquired on the 20th of September 2003 (figure 2). This approach has three major disadvantages:

1. finding GCP on land is not always feasible (e.g. when clouds are present).
2. over a sea scene these GCP has to be on land, and since it is a rubber-sheeting technique the sheet will be fixed, in the best case, from two corners while the other two are flapping with considerable errors on the X and Y directions. The magnitude of this two dimensional error depends on number and distribution of GCP, the extrapolation procedure being employed in the geo-referencing and on the offshore distance (i.e. it increases in the offshore direction).

3. subject to operator error due to the scale difference between a real point on a cartographical map and a grid point of CHRIS image with a minimum size of 900 m².

A better approach would be by using the telemetry data of the PROBA satellite and the geographical coordinates of the observed location to perform geometric correction of the acquired scene by CHRIS on board on PROBA.

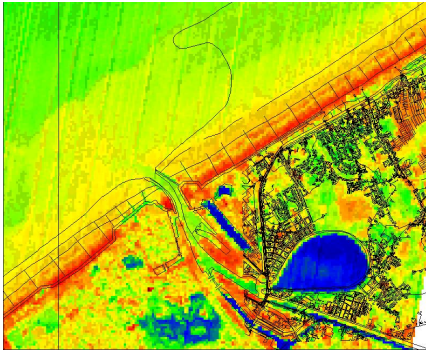


Figure 2. The ground truth cartographical map overlaid on top of the georeferenced CHRIS image.

2.3. Atmospheric correction of CHRIS images

The fly-by-zenith and the minimum-zenith angles of each acquisition were used with satellite altitude and time of overpass to compute the viewing zenith and azimuth angles for a geographical location on the ground.

The data from the sunphotometer fixed at Ostend station were used to estimate the contribution of aerosol scattering to the total recorded radiance at the sensor level.

The water vapor transmittance at 0.94 μm was estimated from the band ratio technique Gao et al. (2000) assuming small variations in the surface reflectance as follows:

$$T(940)_w = \frac{5 \times \rho_t^{(0.94)}}{3 \times \rho_t^{(0.87)}} \quad (1)$$

where $\rho_t^{(\lambda)}$ is the apparent optical quantity at the wavelength λ measured by the sensor. The resulting transmittance is then compared to a look up table of transmittance as a function of water vapor content. The resulting image of water vapor content is shown in figure(3).

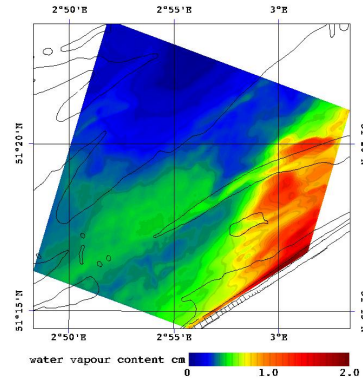


Figure 3. Example of CHRIS byproduct: water vapor content estimated from CHRIS imagery CHRIS0508A.

Atmospheric radiative transfer was then simulated using the second simulation of the satellite signal in the solar spectrum Vermote et al. (1997).

2.4. Vicarious calibration

The objective in this step is to realize the radiometric closure between CHRIS corrected spectra and in-situ measurements. At each band a liner relationship is assumed between CHRIS water leaving reflectance and in-situ measured spectra. The calibration coefficients are then defined to achieve the best fit between the two spectra. The ground-reference sites were divide into calibration and validation sites. Figure (4) shows inter-comparison between the measured spectrum at the validation site st130 and the CHRIS spectrum at the same location. As we can see form figure (4) the relative error between both spectra did not exceed 10%. This is extremely good providing that we have used one site only for the calibration. The results can be improved by having

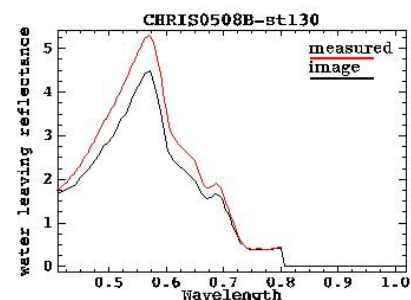


Figure 4. Comparison of image and measured reflectances at st130 (lat: 51.26922 long: 2.89902)

two sites that represent two different water bodies, eventually case 1 and case 2 water. Let us note, however, that the two spectra have the same values of reflectance at the NIR. Therefore SPM can be retrieved from the NIR band ($0.8 \mu\text{m}$) of CHRIS image with high accuracy. Moreover the blue/red ratios have close values in both spectra. In consequence using the band ratio approach to estimate the concentrations of chlorophyll-a from CHRIS image will give close estimates to measured concentration. Upon that the goodness of fit between the measured and CHRIS spectra in the visible range is at its maximum at the blue bands. This feature will increase the accuracy of the retrieved DOM absorption coefficient from the blue bands of CHRIS.

3. HYDRO OPTICAL MODELLING

The water leaving reflectance $\rho_w^{(\lambda)}$ of a uniform radiance field can be related to the inherent optical properties (IOP) as Gordon et al. (1988):

$$\frac{\rho_w^{(\lambda)}}{T_0^{(\lambda)}} = 0.54\pi l_1 \frac{b_b(\lambda)}{b_b(\lambda) + a(\lambda)} \quad (2)$$

Where $l_1 = 0.0949$ is the subsurface expansion coefficients due to internal refraction, reflection and sun zenith. $T_0^{(\lambda)}$ is the solar transmittance from sun-to-target. The absorption $a(\lambda)$ and backscattering $b_b(\lambda)$ coefficients are expressed as:

$$a(\lambda) = a_w(\lambda) + a_{dom}(\lambda) + a_{chla} \quad (3)$$

$$b_b(\lambda) = b_{b(w)}(\lambda) + b_{b(spm)}(\lambda) \quad (4)$$

The subscripts w , dom , $chla$ and spm represent water, dissolved organic matter, chlorophyll-a and suspended particulate matter respectively. Measured values of specific inherent optical properties in the North Sea IVM (1999-2000) will be used to compute the concentration of chlorophyll-a and SPM from retrieved absorption and backscattering coefficients.

For the SPM retrieval we used the NIR band centered at $0.8 \mu\text{m}$ and direct inversion of equation (2), (see figures 5,8 and 11). In this inversion process, other constituents than SPM and water molecules were ignored. The concentrations of chlorophyll-a were retrieved from the single band ratio model of Lee et al. (1996) (see figures 6,9 and 12). Equation (2) was then inverted for DOM having the values of the Chl-a and SPM (see figures 7, 10 and 13).

3.1. maps of marine bio-geophysical quantities in the Belgian coastal waters

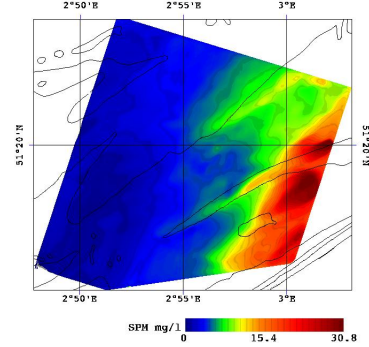


Figure 5. The concentrations of SPM retrieved from CHRIS image acquired on 05/08/2003, FZA=0.

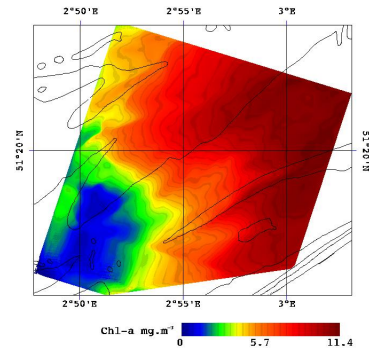


Figure 6. The concentrations of chlorophyll-a retrieved from CHRIS image acquired on 05/08/2003, FZA=0.

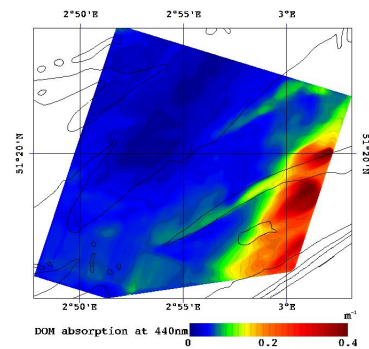


Figure 7. DOM absorption coefficient at $0.44 \mu\text{m}$ retrieved from CHRIS image acquired on 05/08/2003, FZA=0.

The retrieved concentration of SPM (figures 5, 8 and 11) have realistic spatial distribution and ranges of values. The first SPM map (figure 5)

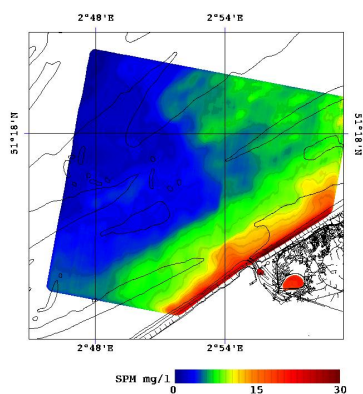


Figure 8. The concentrations of SPM retrieved from CHRIS image acquired on 20/09/2003, FZA=0.

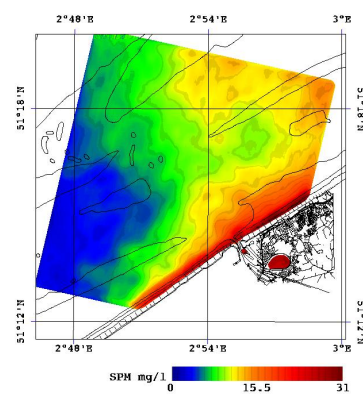


Figure 11. The concentrations of SPM retrieved from CHRIS image acquired on 21/09/2003, FZA=0.

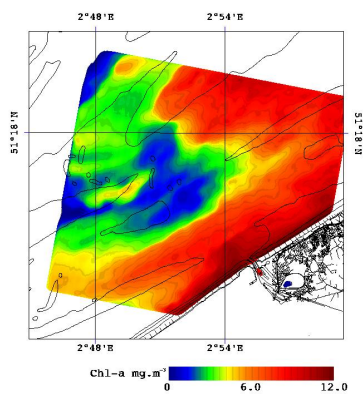


Figure 9. The concentrations of chlorophyll-a retrieved from CHRIS image acquired on 20/09/2003, FZA=0.

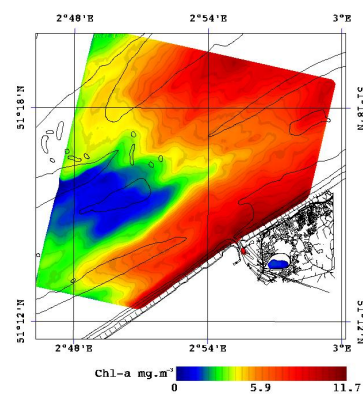


Figure 12. The concentrations of chlorophyll-a retrieved from CHRIS image acquired on 21/09/2003, FZA=0.

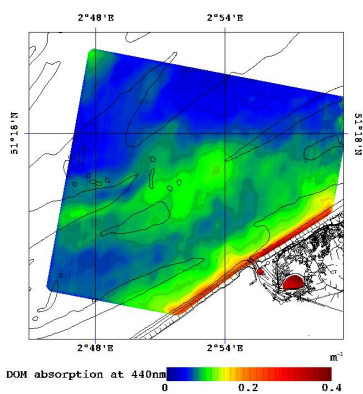


Figure 10. DOM absorption coefficient at 0.44 μm retrieved from CHRIS image acquired on 20/09/2003, FZA=0.

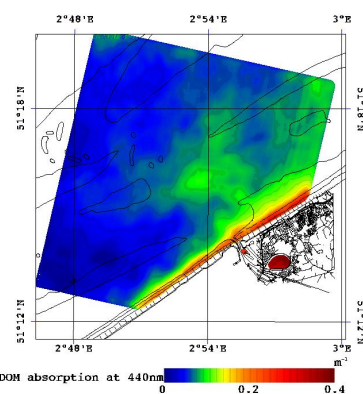


Figure 13. DOM absorption coefficient at 0.44 μm retrieved from CHRIS image acquired on 21/09/2003, FZA=0.

was computed one hour after the ebb-condition. Therefore the concentration of SPM rises from lo-

cal stirring in shallow areas due to the rises of the water level and the interaction of different hy-

drodynamical forces. This is clearly visible along the Wenduinebank sandbank. The other two SPM maps (figures 8 and 11) were computed one and two hours before the ebb-condition, respectively. In this case the tide residual current is still an effective factor in determining the concentration and spatial distribution of SPM. This especially for the SPM map computed two hours before the ebb (figure 11). Here we can see how the interaction of the different hydrodynamical forces is contributing to the magnitude and spatial distribution of SPM along the Belgian coast. In a similar manner the spatial distribution of chlorophyll-a and DOM maps can be explained in the view of the hydrodynamical conditions at the time of image acquisition.

4. CONCLUSION

This paper demonstrated the potential use of CHRIS imagery over water target. It was shown that CHRIS operational processing chain follows those of standard algorithms designed for hyperspectral imagery. In other word CHRIS-imagery in its present status can be used for operational retrieval of marine bio geophysical quantities. The retrieved marine quantities from CHRIS images showed realistic ranges of values. Moreover their spatial distribution were in accordance to what is expected from hydrodynamics simulation at the time of image acquisition. Though improvements are still needed to enhance the quality of the retrieved products. Especially the multi-angularity feature of CHRIS sensor, employing this capability will improve our understanding on the bidirectional effects of the water signal, besides it might provide a better way to correct for the interference of non desirable signals.

5. ACKNOWLEDGEMENT

The authors would like to thank: the European Space Agency (ESA) for providing the opportunity to exploit CHRIS imageries, SIRA for there scientific and technical assistance, Management Unit of Mathematical Models of the North Sea for providing in-situ measurements, Institute for Environmental Studies-Free University of Amsterdam for providing the specific inherent optical properties. The financial support of ESA-PRODEX Experiment Arrangement No. 90018 is gratefully acknowledged.

PUBLISHED WORK IN THE CONTEXT OF CHRIS/PROBA MISSION

1. Salama S. Monbaliu J. and Coppin P., 2004, The atmospheric correction of AVHRR images. *International Journal of Remote Sensing* Vol. 25, No 7-8, 1349-1355
2. Salama S. and Monbaliu J., 2003. Quantification of suspended particulate matters from DAIS/ROSIS images: case-II waters". Third EARSeL workshop on Imaging Spectroscopy, ISBN 2-908885-26-3, pp 423-438.3
3. Salama S., 2003, Optical remote sensing for the estimation of marine bio-geophysical quantities. Ph.D. thesis, ISBN90-5682-437-6
4. Salama S. and Monbaliu J., 2002. Atmospheric correction algorithm for CHRIS images: Application to CASI. *Imaging Spectrometry VIII, Proc. of SPIE, Vol. 4816*, pp 120-131

REFERENCES

- Eisma D., Kalf J., 1979, *Netherlands Journal of Sea Research*, 13, 289
- Gao B., Montes M., Ahmed Z., Davis C., 2000, *Applied Optics*, 39, 887
- Gordon H., Brown O., Evans R., et al., 1988, *Journal of Geophysical Research*, 10909–10924
- Green A.A., Berman M., Switzer P., Craig M.D., 1988, *IEE Transactions on Geoscience and Remote Sensing*, 26, 65
- IVM, 1999-2000, Measurements of the SIOP in the North Sea, institute for Environmental Studies-Free University of Amsterdam, personal communication
- Lee Z., Carder K., Marra J., Steward R., Perry M., 1996, *Applied Optics*, 35, 463
- Vermote E., Tanre D., Deuze J., Herman M., Morcrette J., 1997, *IEEE Transactions on Geoscience and Remote Sensing*, 35, 675